Journal Pre-proof

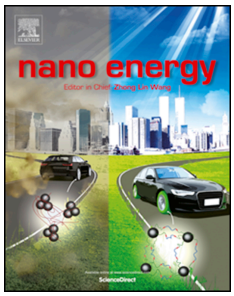

Piezo-phototronic effect on quantum well terahertz photodetector for continuously modulating wavelength

Nian Liu, Gongwei Hu, Minjiang Dan, Ruhao Liu, Yaming Zhang, Lijie Li, Yan Zhang

PII: S2211-2855(19)30798-0

DOI: https://doi.org/10.1016/j.nanoen.2019.104091

Reference: NANOEN 104091

To appear in: *Nano Energy*

Received Date: 26 July 2019

Revised Date: 30 August 2019

Accepted Date: 2 September 2019

Please cite this article as: N. Liu, G. Hu, M. Dan, R. Liu, Y. Zhang, L. Li, Y. Zhang, Piezo-phototronic effect on quantum well terahertz photodetector for continuously modulating wavelength, *Nano Energy* (2019), doi: https://doi.org/10.1016/j.nanoen.2019.104091.

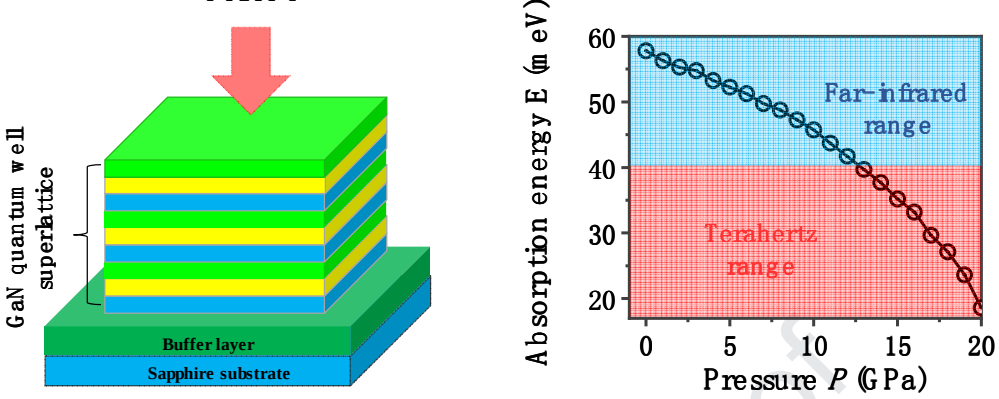

Piezo-phototronic effect has been used to control intersubband optical absorption of GaN-based step quantum well. By employing the self-consistent method of eight-band kp Hamiltonian and Poisson equation, potential profile, absorption spectrum and quantum efficiency are investigated in far-infrared range. Depending on alloy component fraction in AlGaN barrier layer, externally applied strain can effective control absorption peak in Terahertz wavelength. Piezo-phototronic effect provides an effective way for continuously modulate Terahertz photoelectronic devices.

Nian Liu[1,†], Gongwei Hu[1,†], Minjiang Dan[1], Ruhao Liu[1], Yaming Zhang[1], Lijie Li[2,*], and Yan Zhang[1,3,4,*]

[1] *School of Physics, School of Optoelectronic Science and Engineering, University of Electronic Science and Technology of China, Chengdu 610054, China*

[2] *Multidisciplinary Nanotechnology Centre, College of Engineering, Swansea University, Swansea, SA1 8EN, UK*

[3] *CAS Center for Excellence in Nanoscience, Beijing Institute of Nanoenergy and Nanosystems, Chinese Academy of Sciences; National Center for Nanoscience and Technology (NCNST), Beijing 100083, China*

[4] *School of Nanoscience and Technology, University of Chinese Academy of Sciences, Beijing 100049, P. R. China*

[†]Those author contributes equally to this work.

*To whom correspondence should be addressed, E-mail:L.Li@swansea.ac.uk and zhangyan@uestc.edu.cn

Abstract

Piezo-phototronic effect is unique for effectively controlling semiconductor and photonic properties by strain-induced piezoelectric field. In this work, we theoretically explore piezo-phototronic effect on intersubband optical absorption of wurtzite-structured AlGaN/GaN quantum well by self-consistently solving eight-band **kp** Hamiltonian and Poisson equations. Intersubband transition is associated with the transition of two electronic states so it has longer wavelength due to lower transition energy. Strain can also effectively increase absorption wavelength in $Al_{0.15}Ga_{0.85}N/GaN/Al_{0.05}Ga_{0.95}N$ quantum well by quantum Stark effect. For $Al_{0.1}Ga_{0.9}N/GaN/Al_{0.05}Ga_{0.95}N$ quantum well, absorption wavelength decreases with increasing strain. Quantum efficiency can be sensitively controlled by strain. This study not only provides the theory models of piezo-phototronics of intersubband

Keywords: Piezo-phototronic effect, GaN quantum well, intersubband transition, terahertz photodetector

1. Introduction

Piezotronics and piezo-phototronics with the coupling of piezoelectric, semiconductor, and photonic exciton properties in noncentrosymmetric semiconductor materials have received increasing attentions in internet of things and self-powered technology [1-3]. By tuning carrier's generation, recombination and transport, strain-induced piezo-charges play an important role for various high-performance and low-power nanodevices, such as solar cells [4], light-emitting diodes [5], and piezoelectric field-effect transistors [6]. Piezo-phototronic devices have high perfomance and high sensitivity [1, 7, 8]. In addition, piezoelectric field at interface of heterostructure devices can drive a topological phase transition of quantum materials from normal insulator to topological insulator by piezo-phototronic effect [9-11]. Piezotronic and piezo-phototronic effect on quantum materials maybe provide a new way to design ultrahigh performance device, such as topological insulators and spin-transistor devices [12, 13].

Piezo-phototronics involves the process of carrier's generation and recombination which can be controlled by strain-induced piezopotential at the junction region of nanostructured devices [14]. Third generation semiconductors such as ZnO and GaN have a wide band gap over 2.0 eV which greatly limits the optical applications of using piezo-charges on nanojunction regions [15-17]. Previous works had studied piezo-phototronic effect on near infrared range (1.0 μm to 5 μm) [18, 19]. It is important to investigate piezo-phototronic effect on long wavelength applications such as mid-infrared, long wavelength infrared and far-infrared range. For piezo-phototronic devices with the transition between conduction and valence band, the transition energy is greater than the band gap [2, 20].

Quantum well infrared photodetector has novel properties, which depend on intersubband (ISB) transitions. ISB transition devices have large oscillator strengths [21] and

well ISB transitions relieve material limitations of diffusive interfaces and lattice-matched growth requirement [24], holding appealing potential in photodetectors and quantum cascade laster for infrared and terahertz wavelength range.

ISB transition is another important transition process that occurs between two conduction or valence bands [21]. ISB transition has received wide applications in infrared photoelectric devices such as infrared laser, infrared photodetectors and infrared phototransistors [25-28]. ISB electroluminescence had been observed in silicon-based quantum well [29]. In AlInAs/GaInAs quantum well, ISB infrared absorption have observed the existence of electronic bound states with energies higher than the barrier height [30].

Terahertz signals can be generated by ISB transition, which have typical wavelength longer than 30 μm or energy lower than 41 meV. Terahertz has wide applications in secure communications, genetic diagnostics, cancer detections, and cellular scale imaging [31-33]. Quantum cascade laser is typically used for manipulating terahertz signals [34, 35]. Terahertz signal can be modulated by quantum well parameters, such as well width, temperature and doping [36-38]. Although gating voltage is convenient approach to continuously control the wavelength of terahertz devices, the supplied electric field is only in the order of kV/cm which can not modulate the wavelength in a wide range [39-41].

To manipulate the terahertz devices, strong electric field is key factor. Piezoelectric semiconductors, such as GaN and AlN, are good candidates to provide strong electric field by externally applied strain. Piezoelectric field reach up to 10 MV/cm in GaN/InN quantum well, which can drive a topological phase transition from normal insulator to topological insulator [42]. In this work, we provide an effective method for controlling terahertz devices by strain-induced piezo-charges in the AlGaN/GaN step quantum well. Two typical quantum well structures with different barrier material have been studied with externally applied strain. Potential distribution of quantum well, ISB transition energy and transition intensity can be effectively controlled by external applied strain. As a result, absorption spectrum changes in

2. Piezoelectric Field on GaN/AlGaN quantum well

III-V nitrides, such as GaN, AlN and InN have excellent piezoelectric properties for the wurtzite structure. Different from those common semiconductors including GaAs, AlAs and InAs, a sizable electric field resides in the heterojunction material under no externally applied voltage due to the presence of spontaneous and piezoelectric polarization. As a typical example, we focus on the AlGaN/ GaN quantum well structure for demonstrating its characteristics in the terahertz wavelength, as seen in Figure 1(a). Here, we adopt a step quantum well structure with one GaN well layer and two different AlGaN barrier layers with different Al component fractions. This kind of step quantum well is recently proposed both theoretically and experimentally for terahertz photoelectric detection based on the ISB transition [43-45].

In quantum well structure based on wurtzite III-V nitrides, the total polarization includes both the spontaneous polarization P^{sp} and piezoelectric polarization P^{piezo}. Therefore, even if there is no external applied voltage, a strong electric field still appears in the heterostructure system [46, 47]. For a strained quantum well system along *c*-axis direction, the piezoelectric polarization can be expressed as $P^{piezo} = e_{33}s_{33} + e_{31}(s_{11} + s_{22})$, where s_{11}, s_{22} and s_{33} are the strain along *x*, *y* and *z* axis (*c* aixs) direction, e_{33} and e_{31} are the components of piezoelectric coefficient. The total polarization is then written as

$$P_{w,b} = P_{w,b}^{sp} + e_{33,w,b}s_{33,w,b} + e_{31,w,b}\left(s_{11,w,b} + s_{22,w,b}\right), \quad (1)$$

where the subscripts *w* and *b* respectively label the quantity in the well and barrier layer.

For AlGaN and GaN , the strain can be derived inside the well and barrier layer from the stress-strain relation $\sigma = (c)\square(s)$, where c is the elastic coefficient. For simplification, the stress is applied along *z* axis direction, and thus the induced strain can be expressed as $s_{11,b,w}^{ex} = s_{22,b,w}^{ex} = E_{13,b,w}\sigma_{33}$ and $s_{33,b,w}^{ex} = E_{33,b,w}\sigma_{33}$, where E_{13} and E_{33} are the components of E which is the inverse of the elastic coefficient matrix *C*, and σ_{33} is the

Except for external strain, lattice-mismatched strain is also considered. Strain produced by lattice mismatch can be obtained from the relationship $s_{11}^{(0)} = s_{22}^{(0)} = (a_b - a_w)/a_w$, $s_{33}^{(0)} = -2s_{11}^{(0)} C_{13}/C_{33}$ and $s_{12}^{(0)} = s_{23}^{(0)} = s_{31}^{(0)}$, where a_b and a_w are respectively lattice constant of the barrier and well layer, C_{13} and C_{33} are the components of elastic coefficient in wurtzite material. Experimental results suggest that only barrier layer endures the mismatch strain in GaAlN/GaN quantum well [48]. Piezo-phototronic effect is induced by applied strain and lattice mismatch. However, the strain from lattice mismatch is fixed and the applied strain is dynamical, which is primary purpose in this study.

With different layers under external applied strain, the induced polarization field can be written as [49]

$$F_j = \frac{\sum_{k=1}^{3} \left(P_k - P_j\right) L_k / \varepsilon_k}{\varepsilon_0 \varepsilon_j \sum_{k=1}^{3} L_k / \varepsilon_k}, \tag{2}$$

where P_k is the total polarization in *k*-th layer, L_k is the layer width, ε_k is the relative dielectric constant and ε_0 is the vacuum permittivity.

3. Piezo-phototronic Effect on Intersubband Transition and Optical Absorption

Subband energy levels and corresponding wavefunctions are calculated for studying the ISB transition in the step potential well. Typically, conduction band is mostly studied in ISB transition of GaAs/AlGaAs, AlGaN/GaN quantum well [50, 51], which has wide applications. Transition occurring in valence band is strongly dependent on the polarization direction of the incident light, such as TM and TE polarization [52, 53], due to its three *p* orbits in upmost valence band. The downmost conduction band has only one *s* orbit and only TM polarization contributes to the ISB transition, beneficial to the experimental measurement [54]. Considering the electrostatic potential (polarization field), conduction-band discontinuity

case for ISB transition as typical example, the eight band **kp** Hamiltonian matrix is given by [55, 56],

$$H=\begin{pmatrix} G(k) & \Gamma \\ -\bar{\Gamma} & \bar{G}(k) \end{pmatrix}, \tag{3}$$

where G and Γ are 4×4 matrices with the complex conjugate $\bar{G}$ and $\bar{\Gamma}$ respectively. The detailed description of G and Γ matrices is given in Appendix A.

Energy levels and wavefunctions are then obtained by solving Schrödinger equation

$$\left[H\left(k_x=0,k_y=0,k_z=-i\partial_z\right)+V(z)\right]\psi_n(z)=E_n\psi_n(z), \tag{4}$$

where $\psi_n(z)$ is the wave function, E_n is the energy level. $V(z)$ is the potential energy given by $V(z)=-q\phi+\Delta E_c+V_{xc}$, where ϕ is the Hartree potential, $\Delta E_c=0.719\times[E_g(\mathrm{AlGaN})-E_g(\mathrm{GaN})]$ is the band offset at the heterointerface. The exchange-correlation potential V_{xc} is obtained from Refs [57, 58].

Hartree potential is calculated from Poisson equation which is given by [59]

$$\frac{d}{dz}\left[\varepsilon_0\varepsilon_r\frac{d}{dz}-P_z(z)\right]\phi(z)=-q[N_D(z)-n(z)], \tag{5}$$

where N_D is ionized donor concentration, $n(z)$ is free electron concentration.

Schördinger and Poisson equations should be self-consistently solved by an iteration process. To be more specific, given an initial Hartree potential obtained from Eq. (2), the subband energy levels and wave functions can be then calculated from Schördinger equation. Fermi level is subsequently given from charge neutrality condition. Using energy levels, wavefunctions and Fermi energy, one can obtain free electron concentration which is then substituted into Poisson equation to calculate a new Hartree potential. Comparing the updated Hartree potential with the initial value, the iteration process will be terminated if the predefined tolerance (1 mV) is fulfilled for those two Hartree potentials. Otherwise, the iteration proceeds until the convergence condition is met.

exchange-correlation potential V_{xc} [58, 60], free electron concentration $n(z)$ [59], optical absorption coefficient α [61] are given in Appendix A. Here, we set the temperature to be 3 K, and other relevant parameters used in the calculation is listed in TABLE I.

The presented results in this study are mainly focus on the general theory of piezo-phototronic effect on ISB transition. Density function theory (DFT) and quantum molecular dynamics (QMD) maybe the effective method for complex quantum well structure [24, 62].

4. Modify Wavelength of Piezo-phototronic Terahertz Detector by Applied Strain

Terahertz radiation and detection have important applications in secure communications, material identification and genetic diagnostics [31]. Terahertz range is located between infrared and microwave frequencies [63], and has wavelengths from 30 to 300 μm (frequencies from 1 to 10 THz or energy from 4.1 to 41 meV) [64].

Wurtzite GaN and AlN have strong optical phonon absorption in infrared reststrahlen band range [65, 66]. For the E_1 and A_1 phonon modes of GaN and AlN, due to two phonon effect, restrahlen band is broadened approximately into the region of 15-40 THz or 7-25 μm [65, 67], in which the incident light is almost completely absorbed by phonon vibration. However, for the terahertz wavelength, there are strong transmissions between the GaN buffer and sapphire substrate or weak phonon absorption. In addition, stress imposed on the devices will move the optical phonon into higher frequency [68, 69], broadening absorption window to allow a large transmission for the terahertz range. Therefore, it is reasonable and feasible in experiment for terahertz detection using GaN/AlGaN quantum well [43, 45].

Figure 1 shows the schematic of using strain-induced piezoelectric field to control the quantum well potential distribution and further modulate terahertz ISB transition. Figure 1(a) sketches the basic device structure of ISB transition consisting of a superlattice quantum well and GaN buffer layer, both of which are grown on a sapphire substrate. Figure 1(b) shows the enlarged single quantum well structure with and without strain. Gradient color presented here stands for distribution of piezoelectric potential coming from external strain. Figure 1(c)

transition in such step quantum well without external strain. ISB transition occurs between subbands of the conduction bands and interband type involves transitions among conduction-band electrons and valence-band holes. Under an external stress in Figure 1(e), potential profile becomes flattened, and its internal polarization field is reduced. This flattened potential has significant influence on the electronic confinement and energy transition. In the subsequent works, we only focus on ISB transition, because the interband transition has already well studied in various piezo-phototronic devices.

The first device consists of a 3 nm thick $Al_{0.1}Ga_{0.9}N$ space barrier A, a 3 nm thick GaN well layer and a 10 nm thick $Al_{0.05}Ga_{0.95}N$ step barrier B, as shown in Figure 2. Two barrier layers are unintentionally doped with residual n-type concentration 1×10^{17} cm^{-3} and the well layer is n-doped with concentration 1×10^{18} cm^{-3}.

The conduction-band profiles and the corresponding material are shown in Figure 2(a) under the external strain S_{33} varying from 0 to 5.6%, (S_{33} is strain in GaN well layer). It is seen that potential profile in well layer is severely bended by the strong internal polarization field when there is no strain applied on the device. Step barrier B, a key layer for reducing the subband energy level and making transition energy located in terahertz range, has weak electric field with flat potential profile due to the space barrier A which shares those field transmitting from well layer. Distinguished from single quantum well with one barrier and one well layer, step quantum well with three-layer structure (one well and two barriers) can localize the strong polarization field only into two layers, i.e. the well and space barrier layer, benefiting to the rest wide barrier layer responsible for the weak field. This principle is similar to previous studies in terahertz detections based on GaAs single quantum well by setting a wide well layer to reduce quantum size effect under no internal polarized field [64]. Actually, step barrier in our structure can be also viewed as a “pseudo well layer” compared with the space barrier layer because the free electrons are mainly localized in this layer.

Under an external strain, the well-layer potential profile becomes flat due to the

interaction between the free electrons and ionized donors. A weakening of the polarized field in space barrier layer is also observed with the strain increased. The barrier height, no matter in left interface between space barrier and well layer or in right interface between step barrier and space barrier layer, both become higher by deformation potential. The rising of barrier height favors more bound states to be localized in well and step barrier layer, resulting in more bound-bound transitions.

Figure 2(b) shows the absorption spectrum under different strains. With increasing the strain, absorption energy at the peak starts to decrease and then increases at the strain of 1.4%. The peak absorption intensity increases slightly and then decreases. The peak absorption intensity becomes weaker because of the slight bending of potential profile in step barrier. This band bending leads to the asymmetry of structure in step barrier which reduces the overlap of wavefunction as well as the transition possibility. Here, the width of step barrier is much larger than the well layer, and thus the wavefunction of bound states is predominantly localized in the step layer. Notice that since Fermi energy is always located at the energy between ground and first excited state under a fixed doping concentration, only transition from ground state to first excited state has higher strength and lower energy. Following this consideration, only the transition from ground state to first excited state is taken into account throughout the work. Figure 2(c) shows the absorption energy varying with the strain. The energy first decreases slightly, and then increases with the strain increasing. The absorption peak is in the terahertz range at the strain lower than 4.2%, beyond which the absorption energy is out of 10 THz.

Quantum efficiency $QE=1-\exp(-L_w\alpha)$ (L_w is the total width of well and step barrier layer, α is absorption coefficient), a key parameter to evaluate the optical absorption performance of quantum well device, as a function of the strain is shown in Figure 2(d). As we can see, with the increase of the strain, quantum efficiency has a slight increase and then decreases. The reduction of quantum efficiency is due to barrier height that is raised by deformation potential. Accordingly, ground state is gradually shrunk into GaN well layer,

bound states (here it is only ground state) into the well. Such modulation approach of terahertz absorption is featured by continuous manipulation based on piezo-phototronic effect.

Depending on specific structure of quantum well, we can design terahertz photoelectric detection in a flexible fashion. Figure 3 shows another step quantum well with 3 nm $Al_{0.15}Ga_{0.85}N$ space barrier, 3 nm GaN well and 10 nm $Al_{0.05}Ga_{0.95}N$ step barrier. The doping concentration in each layer is the same as in Figure 2. Figure 3(a) shows the conduction-band profiles at different strains. In contrast with Figure 2(a), Figure 3(a) displays an obvious band bending in step barrier layer without strain, which is the result of the polarization imbalance by Al component fraction of two barrier layers [44]. Increasing the strain can drive a tendency from imbalance to balance. This balanced transformation will result in a Stark red shift due to the polarization field, as shown in Figure 3(b). The decrease of absorption energy is completely different from those results mentioned above in Figure 2 where strain increases the absorption energy. Figure 3(c) shows absorption energy as a function of external strain. While the strain reach 3.6%, absorption peak falls into terahertz range. Quantum efficiency is shown with various strain in Figure 3(d). With the strain increasing, quantum efficiency increases first and then maintains almost unchanged. Such unchanged quantum efficiency indicates a saturation of absorption performance by piezo-phototronic effect. Two structures studied above demonstrate a facile modulation of terahertz wavelength by piezo-phototronic effect.

Quantum well devices can obtain high efficiency by superlattice structure. Total absorption efficiency of superlattice device can reach very high, while the number of quantum well is increased [70]. For example, typical value of absorption efficiency of single quantum well is $\eta_1 = 0.3\%$. According to the conventional formula: $1-\exp(-2N\eta_1)$ [70], total absorption efficiency is 50% while the number of quantum well is $N = 115$.

For conventional methods, the absorption wavelengths of terahertz photodetectors are modulated by changing material component, well width and temperature [45, 64, 71]. It is difficult

absorption in a large range by piezo-phototronic effect due to strong piezoelectric field.

In order to investigate the relationships between ISB transition energy, piezoelectric field and deformation potential, absorption spectrum and conduction-band potential profile are shown in Figure 4. The structure parameters and doping are completely the same as in Figure 2. For conveniently seeing the effects of deformation potential and piezoelectric field, we plot the periodic repetition of potential profiles and wavelength functions over two quantum wells. Figure 4(a) shows the modulating results by the piezoelectric field. Deformation potential can induced variation in ISB transition energy and absorption coefficient, as shown in Figure 4(c). Simultaneously combining piezoelectric field and deformation potential can significantly move the absorption peak, as shown in Figure 4(e). To deeply understand the modulating mechanism, we calculate the potential profiles and wavefunctions in Figure 4(b), 4(d) and 4(f). Deformation potential greatly raises band offset at two interfaces (barrier/well interface and well/step-barrier interface), and piezoelectric field tends to flatten potential profile of well layer. When only considering piezoelectric field, ground state and first excited state are always localized at the entire step barrier layer with increasing the strain. A small difference of their wave functions is located at left boundary of narrow well region due to the reduction of polarization field, leading to a slight variation of wave-function overlap and absorption strength. The inconspicuous change of absorption energy is mainly attributed to the effective width that maintains almost unchanged. However, we observe an evident shift of absorption spectrum in Figure 4(b) which is purely originated from deformation potential. To be more specific, deformation potential simultaneously rises the barrier height (or band offset) of three interfaces (barrier/well, well/step barrier, step well/ barrier), and thereby confining more bound states. More importantly, the lift of barrier height at well/step barrier interface makes ground state localized predominantly at the well. This wave function localization on the one hand, reduces the overlap of wave functions and its transition strength, and on the other hand grows the transition energy due to the shrinking of the effective width of ground state. When

absorption energy and reduction of absorption intensity can be observed in the result of two combined effects which are the flattening of the potential profile and the deepening of the well height, as shown in Figure 4(f). The former comes from the piezoelectric field cancelling intrinsic internal polarization of well layer, and the latter is due to the deformation potential rising the interfacial barrier height. Therefore, the nonlinear coupling is the fundamental physics of various high performance piezotronic and piezo-phototronic devices.

Piezo-phototronic effect on GaN-based quantum well structure has been extensively investigated in various optical applications, such as solar cell [73], photoluminescence imaging [74] and optoelectronic devices [75]. In those piezo-phototronic devices, the transitions between electrons and holes in ground state are considered. Comparing with strain-induced strong piezoelectric field, deformation potential has less influence on device performance because it mainly affects high excited state but not ground state by changing the depth of potential well. Therefore, strong piezoelectric field is predominant. For ISB transition devices, the coupling of piezoelectric field and deformation potential will enhance piezo-phototronic effect significantly.

Possible experiments can be designed for above three case by setting proper alloy component fraction to balance either the lattice constant or polarization. The same lattice constant indicates no deformation strain, giving rise to zero deformation potential but limited piezoelectric field. Vegard's law is an effective approach for the adjustment of alloy component fraction to lattice match different materials in experimentally, which has been widely used in III-V group semiconductor quantum wells [76, 77]. Similarly, by properly controlling the alloy composition, polarization field can also be eliminated by matching polarization charges between barrier and well layer [78].

For evaluating the impact of alloy material on the absorption properties of quantum well, we calculate the absorption energy and quantum efficiency as a function of strain and Aluminum component fraction of barrier A layer. Figure 5(a) shows that for relatively large Aluminum component, absorption energy becomes high and exceeds 100 meV. Dashed line gives a smallest absorption energy which increases with the increasing of Aluminum

absorption performance area has also been observed in Figure 3.

5. Conclusion

We theoretically investigate the optical absorption of terahertz range in GaN/AlGaN step quantum well under the influence of externally applied strain. By employing eight-band **kp** model as well as self-consistent solver of Schrödinger equation and Poisson equation, various performance parameters including transition energy, absorption coefficient and quantum efficiency are calculated under two different quantum well structures. Depending on Al component fraction in AlGaN barrier layer, absorption energy and wavelength cab change by externally applied strain. Additionally, quantum efficiency, measuring the absorption performance, exhibits a sensitive strain dependence. Based on simulation results, we further propose two terahertz devices, i.e., low-strain and high-strain terahertz photoelectric detectors, which can realize continuous modulation by the piezo-phototronic effect. Finally, we contrastively explore the respective effect of piezoelectric field and deformation potential on ISB absorption, demonstrating that nonlinear coupling of those two effects leads to performance modulation or sensitivity enhancement in piezo-phototronic devices. This research is expected to pave a wide avenue for piezo-phototronic device applications in far-infrared domain.

Acknowledgements

The authors are thankful for the support from University of Electronic Science and Technology of China (ZYGX2015KYQD063), Swansea University, SPARC II project, and Thousand Talents program for a pioneer researcher and his innovation team, China.

2. Bao, R., et al., *Piezo-phototronic effect on optoelectronic nanodevices.* MRS Bulletin, 2018. **43**(12): p. 952-958.
3. Wang, Z.L., W.Z. Wu, and C. Falconi, *Piezotronics and piezo-phototronics with third-generation semiconductors.* Mrs Bulletin, 2018. **43**(12): p. 922-927.
4. Zheng, D.Q., et al., *High-performance piezo-phototronic solar cell based on two-dimensional materials.* Nano Energy, 2017. **32**: p. 448-453.
5. Yang, Q., et al., *Enhancing light emission of ZnO microwire-based diodes by piezo-phototronic effect.* Nano Lett, 2011. **11**(9): p. 4012-7.
6. Wang, X., et al., *Piezoelectric field effect transistor and nanoforce sensor based on a single ZnO nanowire.* Nano Lett, 2006. **6**(12): p. 2768-72.
7. Yang, Q., et al., *Enhancing sensitivity of a single ZnO micro-/nanowire photodetector by piezo-phototronic effect.* ACS Nano, 2010. **4**(10): p. 6285-91.
8. Wang, Z.L., *Progress in piezotronics and piezo-phototronics.* Adv Mater, 2012. **24**(34): p. 4632-46.
9. Hu, G., et al., *Piezotronic Transistor Based on Topological Insulators.* ACS Nano, 2018. **12**(1): p. 779-785.
10. Dan, M.J., et al., *High performance piezotronic logic nanodevices based on GaN/InN/GaN topological insulator.* Nano Energy, 2018. **50**: p. 544-551.
11. Guo, X., et al., *Quantum information memory based on reconfigurable topological insulators by piezotronic effect.* Nano Energy, 2019. **60**: p. 36-42.
12. Zhang, Y., et al., *Theory of piezotronics and piezo-phototronics.* MRS Bulletin, 2018. **43**(12): p. 928-935.
13. Zhu, L. and Z.L. Wang, *Progress in piezotronics and piezo-phototronics of quantum materials.* Journal of Physics D: Applied Physics, 2019.
14. Zhang, Y. and Z.L. Wang, *Theory of piezo-phototronics for light-emitting diodes.* Adv Mater, 2012. **24**(34): p. 4712-8.
15. Lin, M.E., et al., *Low resistance ohmic contacts on wide band‐gap GaN.* Applied Physics Letters, 1994. **64**(8): p. 1003-1005.
16. Yin, X.L., et al., *MoS2/CdS Nanosheets-on-Nanorod Heterostructure for Highly Efficient Photocatalytic H2 Generation under Visible Light Irradiation.* ACS Appl Mater Interfaces, 2016. **8**(24): p. 15258-66.
17. Huang, S., et al., *Effective Passivation of AlGaN/GaN HEMTs by ALD-Grown AlN Thin Film.* Ieee Electron Device Letters, 2012. **33**(4): p. 516-518.
18. Dai, Y., et al., *Largely Improved Near-Infrared Silicon-Photosensing by the Piezo-Phototronic Effect.* ACS Nano, 2017. **11**(7): p. 7118-7125.
19. Wang, X., et al., *Light-Triggered Pyroelectric Nanogenerator Based on a pn-Junction for Self-Powered Near-Infrared Photosensing.* ACS Nano, 2017. **11**(8): p. 8339-8345.
20. Wang, Z.L., W. Wu, and C. Falconi, *Piezotronics and piezo-phototronics with third-generation semiconductors.* MRS Bulletin, 2018. **43**(12): p. 922-927.
21. West, L.C. and S.J. Eglash, *First observation of an extremely large‐dipole infrared transition within the conduction band of a GaAs quantum well.* Applied Physics Letters, 1985. **46**(12): p.

24. Schmidt, P., et al., *Nano-imaging of intersubband transitions in van der Waals quantum wells.* Nat Nanotechnol, 2018. **13**(11): p. 1035-1041.
25. Scamarcio, G., et al., *High-Power Infrared (8-Micrometer Wavelength) Superlattice Lasers.* Science, 1997. **276**(5313): p. 773-6.
26. Beck, M., et al., *Continuous wave operation of a mid-infrared semiconductor laser at room temperature.* Science, 2002. **295**(5553): p. 301-305.
27. Pesach, A., et al., *Non-polar m-plane intersubband based InGaN/(Al)GaN quantum well infrared photodetectors.* Applied Physics Letters, 2013. **103**(2).
28. Wang, Z., et al., *Charge sensitive infrared phototransistor for 45 μm wavelength.* Journal of Applied Physics, 2010. **107**(9).
29. Dehlinger, G., et al., *Intersubband electroluminescence from silicon-based quantum cascade structures.* Science, 2000. **290**(5500): p. 2277-80.
30. Capasso, F., et al., *Observation of an Electronic Bound-State above a Potential Well.* Nature, 1992. **358**(6387): p. 565-567.
31. Ferguson, B. and X.C. Zhang, *Materials for terahertz science and technology.* Nat Mater, 2002. **1**(1): p. 26-33.
32. Siegel, P.H., *Terahertz technology.* IEEE Transactions on microwave theory and techniques, 2002. **50**(3): p. 910-928.
33. Nagel, M., et al., *Integrated THz technology for label-free genetic diagnostics.* Applied Physics Letters, 2002. **80**(1): p. 154-156.
34. Kohler, R., et al., *Terahertz semiconductor-heterostructure laser.* Nature, 2002. **417**(6885): p. 156-9.
35. Williams, B.S., *Terahertz quantum-cascade lasers.* Nature Photonics, 2007. **1**(9): p. 517-525.
36. Wu, F., et al., *Terahertz intersubband transition in GaN/AlGaN step quantum well.* Journal of Applied Physics, 2013. **113**(15).
37. Graf, M., et al., *Terahertz range quantum well infrared photodetector.* Applied Physics Letters, 2004. **84**(4): p. 475-477.
38. El Fatimy, A., et al., *Terahertz detection by GaN/AlGaN transistors.* Electronics Letters, 2006. **42**(23): p. 1342-1344.
39. Chassagneux, Y., et al., *Electrically pumped photonic-crystal terahertz lasers controlled by boundary conditions.* Nature, 2009. **457**(7226): p. 174-8.
40. Kumar, S., et al., *A 1.8-THz quantum cascade laser operating significantly above the temperature of ħω/kB.* Nature Physics, 2010. **7**(2): p. 166-171.
41. Sirtori, C., S. Barbieri, and R. Colombelli, *Wave engineering with THz quantum cascade lasers.* Nature Photonics, 2013. **7**(9): p. 691-701.
42. Miao, M.S., et al., *Polarization-driven topological insulator transition in a GaN/InN/GaN quantum well.* Phys Rev Lett, 2012. **109**(18): p. 186803.
43. Machhadani, H., et al., *Terahertz intersubband absorption in GaN/AlGaN step quantum wells.* Applied Physics Letters, 2010. **97**(19): p. 191101.
44. Wu, F., et al., *Terahertz intersubband transition in GaN/AlGaN step quantum well.* Journal of

piezoelectric polarization charges in N- and Ga-face AlGaN/GaN heterostructures. Journal of Applied Physics, 1999. **85**(6): p. 3222-3233.

47. Simon, J., et al., *Spontaneous polarization effects inGaN/AlxGa1−xNquantum wells.* Physical Review B, 2000. **61**(11): p. 7211-7214.
48. Grandjean, N., et al., *Built-in electric-field effects in wurtzite AlGaN/GaN quantum wells.* Journal of Applied Physics, 1999. **86**(7): p. 3714-3720.
49. Ridley, B.K., W.J. Schaff, and L.F. Eastman, *Theoretical model for polarization superlattices: Energy levels and intersubband transitions.* Journal of Applied Physics, 2003. **94**(6): p. 3972-3978.
50. Machhadani, H., et al., *Terahertz intersubband absorption in GaN/AlGaN step quantum wells.* Applied Physics Letters, 2010. **97**(19).
51. Sudradjat, F.F., et al., *Far-infrared intersubband photodetectors based on double-step III-nitride quantum wells.* Applied Physics Letters, 2012. **100**(24).
52. Gan, K.-G., et al., *Ultrafast valence intersubband hole relaxation in InGaN multiple-quantum-well laser diodes.* Applied Physics Letters, 2004. **84**(23): p. 4675-4677.
53. Saidi, H., S. Ridene, and H. Bouchriha, *Hole intersubband transitions in wurtzite and zinc-blende strained AlGaN/GaN quantum wells and its interband interaction dependence.* International Journal of Modern Physics B, 2015. **29**(08): p. 1550054.
54. Chuang, S.L. and C.S. Chang, *k·p method for strained wurtzite semiconductors.* Phys Rev B Condens Matter, 1996. **54**(4): p. 2491-2504.
55. Winkelnkemper, M., A. Schliwa, and D. Bimberg, *Interrelation of structural and electronic properties inInxGa1−xN ／GaNquantum dots using an eight-bandk·pmodel.* Physical Review B, 2006. **74**(15).
56. Gershoni, D., C.H. Henry, and G.A. Baraff, *Calculating the optical properties of multidimensional heterostructures: Application to the modeling of quaternary quantum well lasers.* IEEE Journal of Quantum Electronics, 1993. **29**(9): p. 2433-2450.
57. Guo, X.G., et al., *Many-body effects on terahertz quantum well detectors.* Applied Physics Letters, 2009. **94**(20): p. 201101.
58. Bloss, W.L., *Effects of Hartree, exchange, and correlation energy on intersubband transitions.* Journal of Applied Physics, 1989. **66**(8): p. 3639-3642.
59. Sacconi, F., et al., *Spontaneous and piezoelectric polarization effects on the output characteristics of AlGaN/GaN heterojunction modulation doped FETs.* IEEE Transactions on Electron Devices, 2001. **48**(3): p. 450-457.
60. Guo, X.G., et al., *Many-body effects on terahertz quantum well detectors.* Applied Physics Letters, 2009. **94**(20).
61. Chuang, S.L., *Optical gain of strained wurtzite GaN quantum-well lasers.* IEEE Journal of Quantum Electronics, 1996. **32**(10): p. 1791-1800.
62. Strak, P., et al., *Principal physical properties of GaN/AlN multiquantum well systems determined by density functional theory calculations.* Journal of Applied Physics, 2013. **113**(19): p. 193706.

65. Yang, J.Y., et al., *Photon absorption in the Restrahlen band of thin films of GaN and AlN: Two phonon effects.* Journal of Applied Physics, 2005. **98**(4).
66. Kucharski, R., et al., *Transparency of Semi-Insulating, n-Type, and p-Type Ammonothermal GaN Substrates in the Near-Infrared, Mid-Infrared, and THz Spectral Range.* Crystals, 2017. **7**(7).
67. Kandaswamy, P.K., et al., *Midinfrared intersubband absorption in GaN/AlGaN superlattices on Si(111) templates.* Applied Physics Letters, 2009. **95**(14): p. 141911.
68. Wagner, J.M. and F. Bechstedt, *Pressure dependence of the dielectric and lattice-dynamical properties of GaN and AlN.* Physical Review B, 2000. **62**(7): p. 4526-4534.
69. Goñi, A.R., et al., *Effect of pressure on optical phonon modes and transverse effective charges inGaNandAlN.* Physical Review B, 2001. **64**(3).
70. Liu, H.C., et al., *High absorption (>90%) quantum-well infrared photodetectors.* Applied Physics Letters, 2001. **79**(25): p. 4237-4239.
71. Muravjov, A.V., et al., *Temperature dependence of plasmonic terahertz absorption in grating-gate gallium-nitride transistor structures.* Applied Physics Letters, 2010. **96**(4): p. 042105.
72. Mii, Y.J., et al., *Large Stark shifts of the local to global state intersubband transitions in step quantum wells.* Applied Physics Letters, 1990. **56**(20): p. 1986-1988.
73. Jiang, C., et al., *Enhanced Solar Cell Conversion Efficiency of InGaN/GaN Multiple Quantum Wells by Piezo-Phototronic Effect.* ACS Nano, 2017. **11**(9): p. 9405-9412.
74. Peng, M., et al., *High-resolution dynamic pressure sensor array based on piezo-phototronic effect tuned photoluminescence imaging.* ACS Nano, 2015. **9**(3): p. 3143-50.
75. Huang, X., et al., *Piezo-Phototronic Effect in a Quantum Well Structure.* ACS Nano, 2016. **10**(5): p. 5145-52.
76. Gonschorek, M., et al., *High electron mobility lattice-matched AlInN ／GaN field-effect transistor heterostructures.* Applied Physics Letters, 2006. **89**(6): p. 062106.
77. Butte, R., et al., *Current status of AlInN layers lattice-matched to GaN for photonics and electronics.* Journal of Physics D-Applied Physics, 2007. **40**(20): p. 6328-6344.
78. Schubert, M.F., et al., *Polarization-matched GaInN ／AlGaInN multi-quantum-well light-emitting diodes with reduced efficiency droop.* Applied Physics Letters, 2008. **93**(4): p. 041102.
79. Vurgaftman, I. and J.R. Meyer, *Band parameters for nitrogen-containing semiconductors.* Journal of Applied Physics, 2003. **94**(6): p. 3675-3696.
80. Vurgaftman, I., J.R. Meyer, and L.R. Ram-Mohan, *Band parameters for III–V compound semiconductors and their alloys.* Journal of Applied Physics, 2001. **89**(11): p. 5815-5875.
81. Honig, G., et al., *Manifestation of unconventional biexciton states in quantum dots.* Nat Commun, 2014. **5**: p. 5721.
82. Rinke, P., et al., *Consistent set of band parameters for the group-III nitrides AlN, GaN, and InN.* Physical Review B, 2008. **77**(7).
83. Grandjean, N., J. Massies, and M. Leroux, *Self-limitation of AlGaN/GaN quantum well energy*

Figure 1. Schematic of using piezo-phototronic effect to control terahertz photoelectric devices. (a) Device structure consisting of substrate, buffer layer and quantum wells superlattice. (b) Basic structure of a single quantum well with and without strain. Gradient color shown in the quantum well under strain signifies strain-induced piezoelectric potential distribution. (c) In-plane energy band dispersion of wurtzite GaN bulk material. Heavy hole (HH), light hole (LH) and crystal-field split-off hole (CH) are presented in the valence band. Potential profile, ISB transition, interband transition and electron/hole wave functions without (d) and with (e) the strain. Externally applied strain is along *c* axis direction.

Figure 2. (a) Strain dependent conduction-band potential profiles. (b) Absorption spectrum of quantum well devices. (c) Absorption energy versus the strain. (d) Maximum *QE* at absorption peak against the strain. Quantum well is composed by a 3 nm thick $Al_{0.1}Ga_{0.9}N$ space barrier, a 3 nm thick GaN well layer and a 10 nm thick $Al_{0.05}Ga_{0.95}N$ step barrier layer. Space barrier and step barrier are unintentional n-doping 1×10^{17} cm^{-3}, and well layer is n-doping 1×10^{18} cm^{-3}.

Figure 3. The same performance measurements as in Figure 2 but for different quantum well structure. Except for a change that Al mole compositions in space barrier tunes to 15%, other parameters are the same as in Figure 2. (a) Strain dependent conduction-band potential profiles. (b) Absorption spectrum. (c) Absorption energy versus the strain. (d) Maximum *QE* as a function of the strain.

Figure 4. Comparisons of piezoelectric field and deformation potential from absorption spectrum (a) (c) (e) and potential profile (b) (d) (f). (a) and (b) are the cases with piezoelectric field but no deformation potential. (c) and (d) are the case with deformation potential but without piezoelectric field. (e) and (f) are the case combining those two effects.

with best performance. Here, Aluminium fraction y of step barrier B is fixed at 0.05.

[79-82]. For $Al_xGa_{1-x}N$ alloy material, the parameter A takes linear interpolation form $A(Al_xGa_{1-x}N) = xA(AlN) + (1-x)A(GaN)$ except for the bandgap E_g and spontaneous polarization P_{sp}, which should consider the bowing parameter C via the relationship $B(Al_xGa_{1-x}N) = xB(AlN) + (1-x)B(GaN) - Cx(1-x)$. Here, the bowing parameters are 0.7 eV and -0.021 C/m^2 for the bandgap and spontaneous polarization, respectively [83].

parameter	GaN	AlN	parameter	GaN	AlN
a(Å)	3.189	3.112	A_2	-0.528	-0.311
c(Å)	5.185	4.892	A_3	5.414	3.671
C_{11}(GPa)	390	396	A_4	-2.512	-1.147
C_{12}(GPa)	145	137	A_5	-2.510	-1.329
C_{13}(GPa)	106	108	A_6	-3.202	-1.952
C_{33}(GPa)	398	373	A_7（eV·Å）	0.046	0.026
C_{44}(GPa)	105	116	a_1(eV)	-4.9	-3.4
e_{33}(C/m^2)	1.23	1.79	a_2(eV)	-11.3	-11.8
e_{31}(C/m^2)	-0.35	-0.50	D_1(eV)	-3.7	-17.1
P_{sp}(C/m^2)	-0.034	-0.090	D_2(eV)	4.5	7.9
ε_r	9.8	9.1	D_3(eV)	8.2	8.8
α(meV/K)	0.909	1.799	D_4(eV)	-4.1	-3.9
β(K)	830	1462	D_5(eV)	-4.0	-3.4
E_G(eV)	3.510	6.25	D_6(eV)	-5.5	-3.4
Δ_{SO}（eV）	0.017	0.019	c_{13}(dyn/cm^2)	15.8×10^{11}	12.0×10^{11}
Δ_{CR}（eV）	0.010	-0.169	c_{33}(dyn/cm^2)	26.7×10^{11}	39.5×10^{11}
$m_{\|\|}/m_0$	0.186	0.322	E_{p1}(eV)	17.292	16.972
$m_{\perp}/m_0$	0.209	0.329	E_{p2}(eV)	16.262	18.165
A_1	-5.947	-3.991			

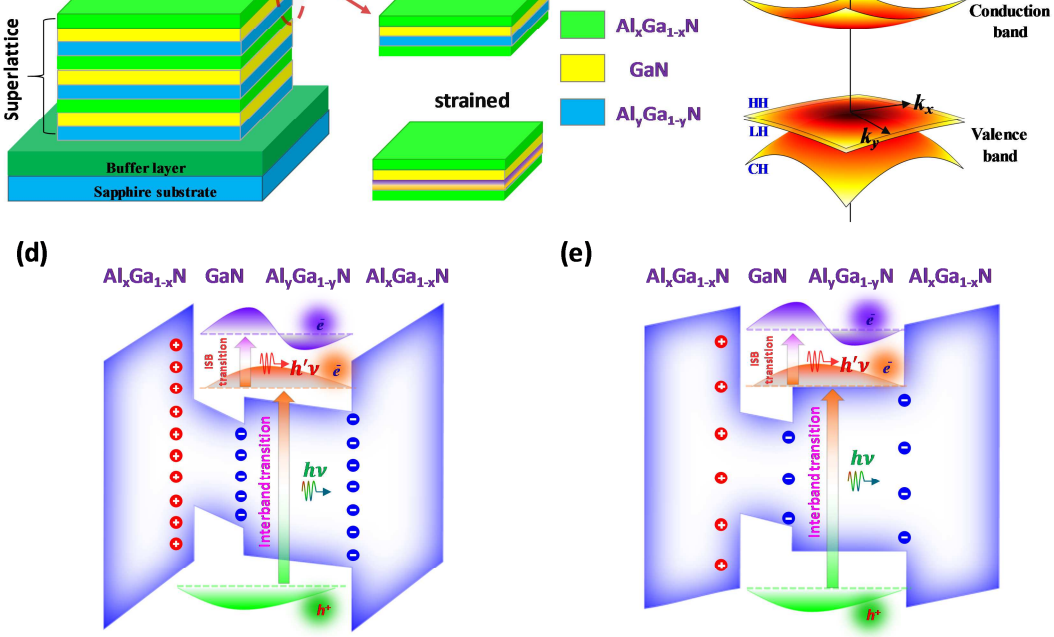

Figure 1

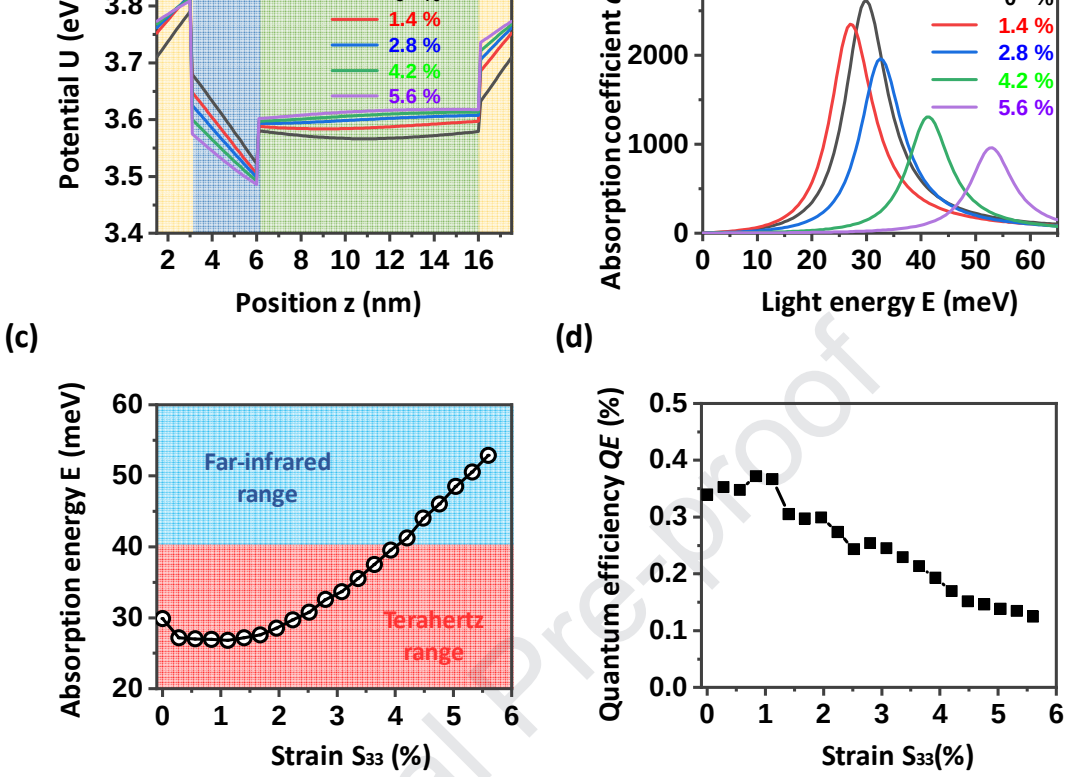

Figure 2

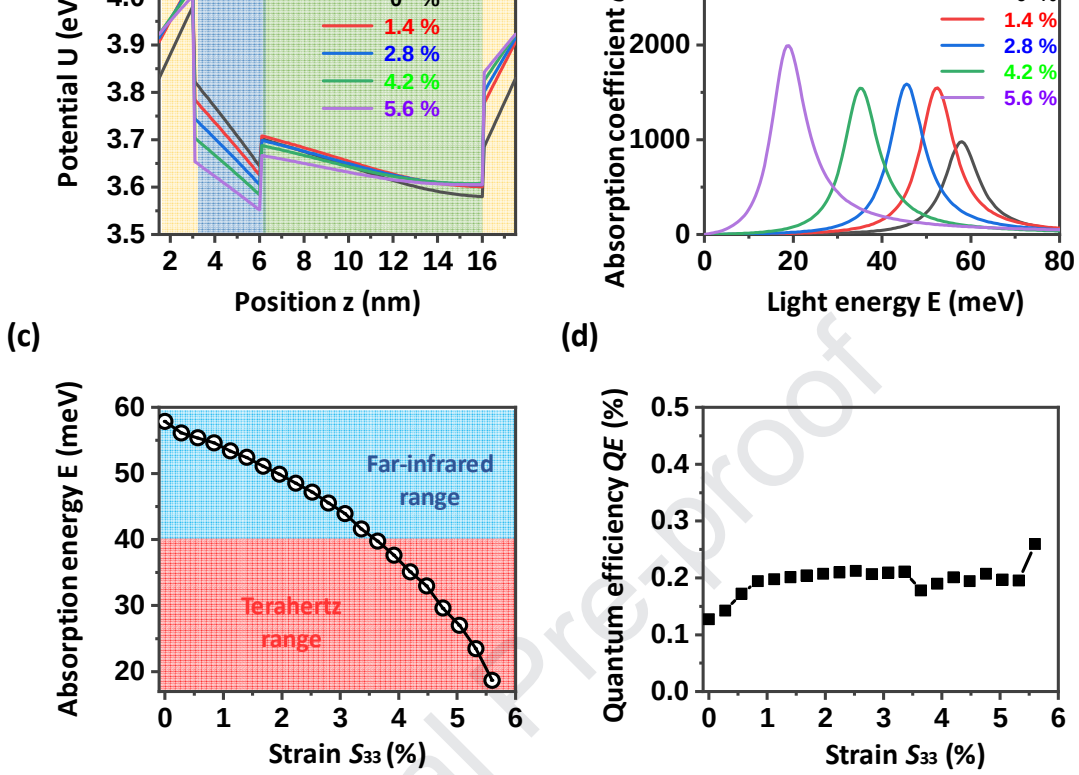

Figure 3

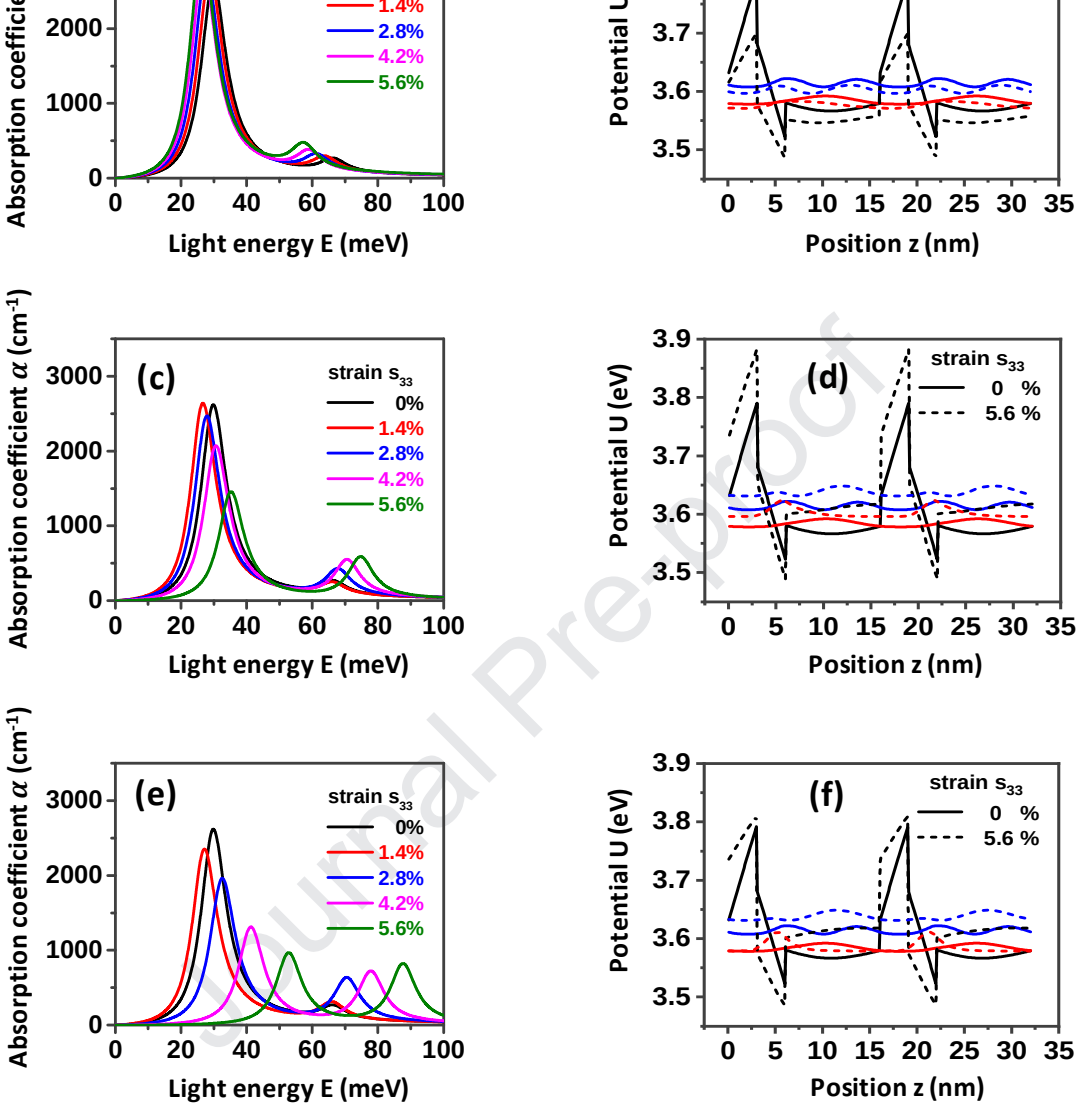

Figure 4

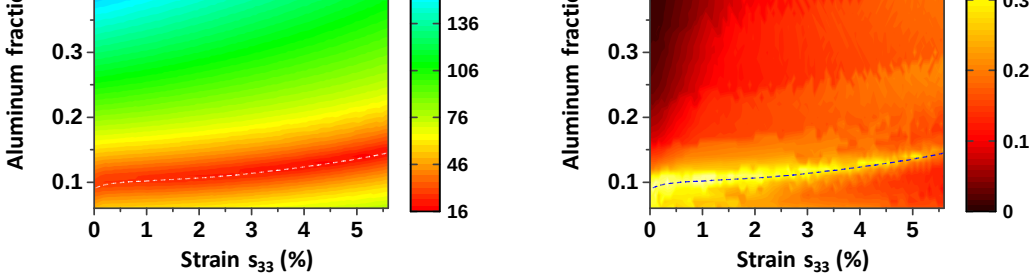

Figure 5

3. Piezo-phototronic effect offer an effective way to continuously modulate wavelength of Terahertz photodetectors.